One- and two-dimensional solitons in second-harmonic-generating lattices

Boris A. Malomed,[1] P. G. Kevrekidis,[2,*] D. J. Frantzeskakis,[3] H. E. Nistazakis,[3] and A. N. Yannacopoulos[3]
[1]*Department of Inderdisciplinary Studies, Faculty of Engineering, Tel Aviv University, Tel Aviv 69978, Israel*
[2]*Department of Mathematics and Statistics, University of Massachusetts, Lederle Graduate Research Tower, Amherst, Massachusetts 01003-4515*
[3]*Department of Physics, University of Athens, Panepistimiopolis, GR 157 84 Athens, Greece*
(Received 16 November 2001; revised manuscript received 24 January 2002; published 30 April 2002)

In a model of a dynamical lattice with the on-site second-harmonic-generating nonlinearity and harmonic intersite couplings (that may be equal or different for the fundamental and second harmonics), various solitary-wave solutions are considered in one and two dimensions (1D and 2D). Fundamental (single-hump) solitons are identified in either dimension and their stability is examined and compared to previous results as well as to what is known for the model's continuum counterpart. Stability limits in terms of the coupling constants, which depend on the value of the phase-mismatch parameter, are found for solitons of the twisted-mode type in the 1D lattice, and for their counterparts of two different types (one being a discrete vortex) in the 2D lattice. When the twisted-mode soliton is unstable, the instability, which may be either oscillatory or due to imaginary eigenfrequency pairs, transforms the unstable soliton into a stable fundamental one, in both 1D and 2D cases.

DOI: 10.1103/PhysRevE.65.056606 PACS number(s): 63.20.Pw

I. INTRODUCTION

Dynamics of localized states (''discrete solitons,'' i.e., intrinsic localized modes, ILMs) in nonlinear dynamical lattices, both one and two dimensional (1D and 2D), have been attracting a great deal of interest, starting from the works in Refs. [1,2], where basic types of ILMs were predicted for 1D lattices. A review of the ILM dynamics was given in Ref. [3] (see also the paper [4]) and more recently in Ref. [5]. ILMs were observed in a number of recent experiments, including localized spin-wave excitations in quasi-1D antiferromagnets [6], complex electronic materials such as halide-bridged transition-metal complexes [7], coupled optical-waveguide arrays [8,9], and Josephson ladders [10,11].

Quite commonly, models supporting ILMs assume lattices with harmonic intersite interactions and an on-site quartic potential. By means of the rotating-wave approximation, these models can be reduced to the discrete nonlinear Schrödinger (DNLS) equation. Besides that, the DNLS equation finds direct applications in modeling arrays of nonlinear optical fibers [12] and waveguides [8,9] and other systems such as, for instance, long biological molecules (see, e.g., Ref. [13] and references therein). The study of ILMs and their stability in the DNLS equation(s) is facilitated by the fact that ILMs are then represented by stationary solutions.

Fewer works considered another physically relevant model of an optical-waveguide array, in which the nonlinearity is quadratic, representing the second-harmonic generation (SHG). Among the first results for ILMs in discrete SHG systems were those reported in Ref. [14] (see also a review [15] on solitons in SHG media, which includes a section describing solitons in discrete systems). Besides the optical-waveguide arrays with quadratic nonlinearity, the same model may describe dynamics of Fermi-resonance interface modes in multilayered systems based on organic crystals [16]. Further studies have revealed 1D, 2D, and 3D strongly localized solitons in the latter system, of both bright (''peak'' and ''crater'') and dark types, see Refs. [17] and references therein; interestingly, some types of the multidimensional solitons in that model have no 1D analogs in the same system. A similar model applies to a nonlinear dynamical lattice with the on-site quadratic nonlinearity of a general form [18].

It is relevant to mention that physical models of coupled SHG waveguides were studied in detail in Ref. [19]. In that work, various dynamical states were analyzed for the case of a ''monomer'' (a single waveguide) and a ''dimer'' (two coupled waveguides). SHG systems embedded in linear layered structures have also recently been used to design a quadratic nonlinear photonic crystal and study discrete solitary waves in it [20].

The aim of the present work is to present results of a systematic study of the existence and stability of various types of ILMs in 1D and 2D SHG dynamical lattices. In the 1D case, we find the fundamental (single-humped) and the so-called twisted-mode solitons. In this case, our findings partly overlap with results that were presented, in a sketchy form, in Ref. [14], but most results were not presented elsewhere before (to the best of our knowledge). We also report detailed results for the 2D lattices, including fundamental solitons, twisted modes, as well as solitons with intrinsic vorticity (for the DNLS equation in two dimensions with the cubic nonlinearity, the existence of discrete solitons with vorticity is a well-established fact; see e.g., [21,22] and references therein). We find that the fundamental solitons are, most typically (for the parameter ranges considered herein), stable in either dimension. However, instabilities of such solutions do occur and have also been identified. Topologically charged solitons, i.e., the twisted-mode ones in 1D and 2D, as well as genuine vortex solitons in 2D, always have stabil-

*Corresponding author. FAX: (413)-545-1801. Email address: kevrekid@math.umass.edu

ity borders. These conclusions are in line with the known facts that the fundamental solitons are, in most cases, stable in the continuum limit, while the twisted solitons are always unstable in the same limit.

II. THE MODEL

The description of the parametric interaction (mutual conversion) between the fundamental-frequency (FF) waves $\psi_n(t)$ and their second-harmonic (SH) counterparts $\phi_n(t)$ in an array of SHG waveguides with one discrete spatial dimension is based on the coupled equations

$$i\frac{\partial}{\partial t}\psi_n = -C_1\Delta_2\psi_n - \psi_n^*\phi_n, \tag{1}$$

$$2i\frac{\partial}{\partial t}\phi_n = -C_2\Delta_2\phi_n - \psi_n^2 - k\phi_n, \tag{2}$$

where $\Delta_2\psi_n = \psi_{n+1} + \psi_{n-1} - 2\psi_n$ is the discrete Laplacian with unit spacing, $C_{1,2}$ are the FF and SH lattice-coupling constants, and k is the mismatch parameter. It should be noted that, in the case of the waveguide array, t has the meaning of propagation distance, rather than time.

In some works (in particular, in Ref. [14]), the basic equations were taken in a slightly different form, without the factor of 2 in front of the time derivative in Eq. (2),

$$i\frac{\partial}{\partial t}\psi_n = -C_1\Delta_2\psi_n - \psi_n^*\phi_n, \tag{3}$$

$$i\frac{\partial}{\partial t}\phi_n = -C_2\Delta_2\phi_n - \psi_n^2 - k\phi_n. \tag{4}$$

This difference may be essential if the coupling constants $C_{1,2}$ are fixed independently. In this connection, we notice that, in the continuum limit, i.e., as $C_{1,2}\to\infty$, the ratio C_1/C_2 is equal to the ratio of the diffraction coefficients, which are the same for both harmonics [15]. Therefore we will, chiefly, consider the case $C_1 = C_2$ in Eqs. (1) and (2). Nevertheless, the couplings between discrete waveguides in the array may depend on the carrier wavelength, therefore C_1 and C_2 may be different (in that case, one should expect that $C_2 \leqslant C_1$). To be completely accurate, we note that in [14], Eq. (3) also had a factor of 2 in front of the last term in the equation; however, the latter factor can be easily removed by a rescaling.

Note that, if the equations are taken in the form of Eqs. (3) and (4), rather than Eqs. (1) and (2), and it is fixed that $C_1 = C_2$, this is readily shown to be tantamount to taking Eqs. (1) and (2) with $C_2 = C_1/2$, which is also a physically meaningful case, as it complies with the above-mentioned restriction $C_2 < C_1$. We have checked that results for the stability of solitons, if obtained from Eqs. (3) and (4), turn out to be similar to those that will be displayed below for Eqs. (1) and (2) (when, nevertheless, there are differences, they will be pointed out).

Equations (1) and (2) conserve two dynamical invariants, namely, the Hamiltonian

$$H = \sum_n \left[C_1|\psi_n - \psi_{n-1}|^2 + \frac{1}{2}C_2|\phi_n - \phi_{n-1}|^2 - \frac{1}{2}\psi_n^2\phi_n^* - \frac{1}{2}(\psi_n^*)^2\phi_n - \frac{1}{2}k|\phi_n|^2 \right]$$

(where the asterisk stands for complex conjugation) and the net power $P \equiv 2P_1 + P_2$, where the FF and SH powers are

$$P_1 = \sum_n |\psi_n|^2, \quad P_2 = \sum_n |\phi_n|^2. \tag{5}$$

If Eqs. (3) and (4) are used instead of Eqs. (1) and (2), the conserved net power is $P_1 + P_2$.

We will consider stationary solutions exponentially localized in both FF and SH components, which have the form

$$\psi_n(t) = \exp(i\Lambda t)u_n, \quad \phi_n(t) = \exp(2i\Lambda t)v_n. \tag{6}$$

Once the stationary solutions are identified (by means of numerically performed Newton iterations), stability analysis around them is performed by solving the eigenvalue problem for a perturbed solution, which is sought for in the form

$$\psi_n(t) = \exp(i\Lambda t)[u_n + a_n\exp(i\omega t) + b_n\exp(-i\omega^* t)], \tag{7}$$

$$\phi_n(t) = \exp(2i\Lambda t)[v_n + c_n\exp(i\omega t) + d_n\exp(-i\omega^* t)], \tag{8}$$

where ω is the (complex, in the general case) eigenfrequency, a_n, b_n, c_n, and d_n being infinitesimal amplitudes of the perturbation. The linearized equations for the perturbations, as derived from Eqs. (1) and (2), are

$$-\omega a_n = -C_1\Delta_2 a_n - u_n^* c_n - v_n b_n^* + \Lambda a_n, \tag{9}$$

$$\omega b_n^* = -C_1\Delta_2 b_n^* - u_n d_n^* - v_n^* a_n + \Lambda b_n^*, \tag{10}$$

$$-2\omega c_n = -C_2\Delta_2 c_n - 2u_n a_n - kc_n + 4\Lambda c_n, \tag{11}$$

$$2\omega d_n^* = -C_2\Delta_2 d_n^* - 2u_n^* b_n^* - kd_n^* + 4\Lambda d_n^*. \tag{12}$$

The latter must be solved with the boundary conditions stating that the perturbation eigenmodes remain bounded (or vanish) as $|n|\to\infty$.

III. ONE-DIMENSIONAL SOLITONS AND THEIR STABILITY

A. Fundamental solitons

It is easy to find a family of fundamental-soliton solutions, in which both the FF and SH components are represented by single-humped pulses. One can easily create this solution branch, starting from the anticontinuum (AC) limit, $C_{1,2} = 0$. In this limit, the fields are different from zero at a single lattice site $n = n_0$, where

$$v_{n_0} = \Lambda, \quad u_{n_0} = \sqrt{(2\Lambda - k)v_{n_0}}. \tag{13}$$

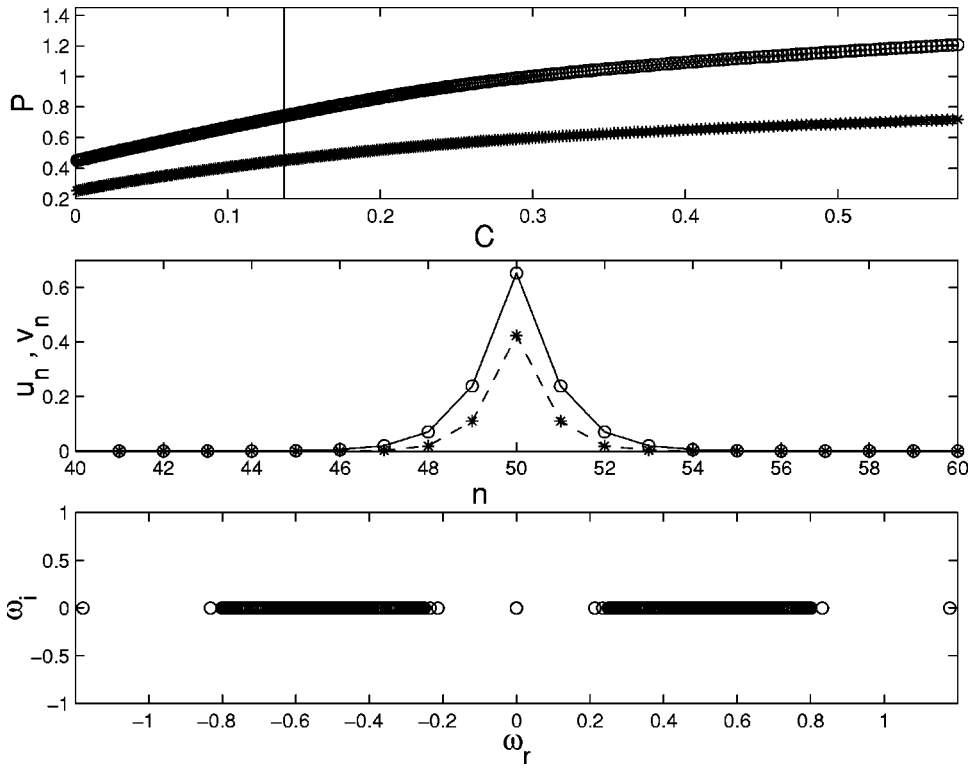

FIG. 1. Fundamental (single-humped) solitons in the discrete SHG model for $k=0.2$ and $\Lambda=0.25$. The results shown in this figure and in Fig. 2 were obtained for Eqs. (1) and (2). In other figures, we used Eqs. (3) and (4), unless explicitly stated otherwise. The top panel shows the norm of the FF (circles) and SH (stars) fields vs the coupling constant $C_1=C_2\equiv C$. The middle panel shows an example of the solution (FF and SH components are shown, respectively, by circles and stars) for $C=0.1368$ (which corresponds to the vertical line in the top panel). The bottom panel shows the corresponding eigenfrequencies; ω_r and ω_i stand for their real and imaginary parts, respectively. The soliton is stable, as there are no eigenfrequencies with $\omega_i \neq 0$.

These solutions continue to exist as discrete solitons at finite $C_{1,2}$, which may be stable according to Ref. [14] (although the eigenvalues were not computed in that work), and they go over into the well-known fundamental SHG solitons in the continuum limit, $C_{1,2}\to\infty$, most of which are stable in the rigorous sense [15,23].

As it was mentioned above, we set $C_1=C_2=C$ in the computations, unless stated otherwise. Using the scaling invariance of the equations, we fixed the frequency, setting $\Lambda=0.25$ in most cases, and varied C, starting from the AC limit, $C=0$ [see Eqs. (13)]. Nevertheless, the persistence of the basic phenomenology was verified by varying Λ as well.

The branch of the fundamental-soliton stationary solutions is displayed in Fig. 1. The top panel in the figure shows the FF (circles) and SH (stars) powers, defined in Eq. (5), as functions of the coupling C. An example of the FF and SH solitary waves is shown, for $C=0.1368$ (corresponding to the vertical line in the top panel), in the middle panel of the figure.

The eigenfrequencies produced by the linearized equations for the particular soliton solution shown in the middle panel of Fig. 1 are presented in the lower panel of the figure, which displays the spectral plane (ω_r,ω_i) of the eigenfrequencies $\omega\equiv\omega_r+i\omega_i$. Infinitesimal delocalized perturbations $\sim\exp(iqn)$ give rise to two continuous bands in the spectrum of small perturbations around the soliton. The continuous bands are parametrized by the perturbation wave number q, according to the dispersion relations

$$\omega=\pm[\Lambda+2C(1-\cos q)], \tag{14}$$

$$\omega=\pm\left[2\Lambda-\frac{k}{2}+C(1-\cos q)\right]. \tag{15}$$

If Eqs. (3) and (4) are used instead of Eqs. (1) and (2), then Eq. (15) takes the form $\omega=\pm[2\Lambda-k+2C(1-\cos q)]$. The absence of any isolated eigenfrequency with a nonzero imaginary part in the lower panel of Fig. 1 confirms the linear stability of the fundamental soliton.

Notice, however, the presence of isolated real eigenfrequencies in Fig. 1, which correspond to *internal modes* of the soliton. These have bifurcated from the edges of the continuous spectrum (CS). The existence of such modes is an important fact. In the continuum limit, internal modes in SHG solitons were studied in detail in Refs. [23,24]. In Fig. 2, we display the internal-mode eigenfrequencies of the soliton, found in the present discrete model as functions of the coupling constant. The top panel of the figure shows the modes bifurcating from the upper edge of CS. The solid line corresponds to an internal mode, which survives even in the continuum limit [24], while the dashed line indicates a mode that bifurcates from the upper edge of one CS band, but is then eventually absorbed by the upper edge of the other band, see Eqs. (14) and (15). The solid line corresponds to an even-parity mode, while the opposite is true for the dashed line. The amplitudes of the corresponding eigenvectors are of comparable amplitude in their FF and SH components (however the amplitude of the SH has been found to be slightly larger than that of the FF in our numerical computations). Note that the upper edges of the two bands (14) and (15), corresponding to $\cos q=-1$, cross each other at $2C=\Lambda-k/2$.

In the bottom panel of Fig. 2, the eigenfrequencies of internal modes bifurcating from the lower edge of the continuous spectrum are shown. The eigenmode associated with the eigenfrequency depicted by the solid line in this panel is analogous to the so-called pinning or translational eigen-

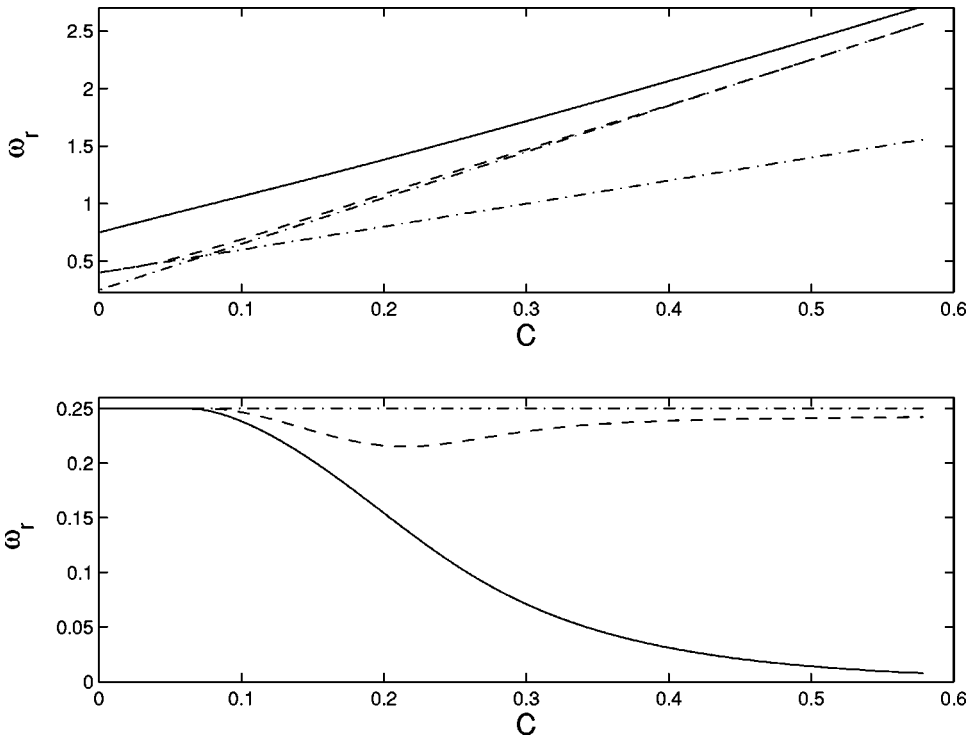

FIG. 2. The internal modes' eigenfrequencies as functions of C for the fundamental solitons. The top panel pertains to the modes that are close to the top edge of the upper band of the continuous spectrum [the upper edges of the continuous bands, given by Eqs. (14) and (15), are shown by the dashed-dotted lines]. The solid line corresponds to a genuine internal mode, which lies outside the bands for all the values of C. The dashed line shows a mode that bifurcates from the top edge of the upper band and is eventually absorbed by the top edge of the lower band. The bottom panel shows the bottom edge of the lower band of the continuous spectrum $\omega=\Lambda$ (dash-dotted line) and the frequencies of the bifurcating "pinning" (solid line) and "breathing" (dashed line) modes as a function of C. $k=0.2$.

mode, which is well known for solitons in 1D dynamical lattices with cubic nonlinearity. Similarly, the eigenmode associated with the eigenfrequency shown by the dashed line is the counterpart of the breathing or edge mode, which is known in the cubic case [25,26]. As is expected from the Sturm-Liouville theory, the pinning mode for a fundamental soliton will have an antisymmetric spatial profile (odd parity), while the opposite will be true for the even-parity breathing mode.

On the basis of a large body of numerical results, we have concluded that the fundamental (single-humped) branch of the soliton solutions is, in the typical range of parameters used herein, most commonly stable. Comparing this result with the known results for the stability of the 1D fundamental $\chi^{(2)}$ solitons in the continuum limit, it is relevant to mention that the latter solitons are known to be unstable, in terms of our notation, at large positive values of k [23,24]. This prompted us to search for a similar instability in the discrete model as well. Indeed, we have found that for values of k larger than those typically studied here, instability of the fundamental soliton does occur in the discrete model also. An example of this is given in Fig. 3, where the evolution of the fundamental-soliton solution is shown as a function of k for $C=0.05$. It has been found that for $k\approx 0.456$ (the rightmost point in the top panel of Fig. 3, whose spatial profile and eigenfrequencies are shown in the middle and bottom panels, respectively), the branch becomes unstable. The instability arises due to a pair of eigenfrequencies (that have bifurcated from the continuous spectrum) that become imaginary as k increases. The bifurcating mode is the even-parity breathing mode. This scenario is typically observed in the evolution of the fundamental branch following the variation of the mismatch parameter and is analogous to that observed in the continuum version of the model [23,24].

B. Twisted-mode solitons

We now turn to the so-called twisted-localized-mode (TLM) solutions. These were originally investigated in models with the cubic nonlinearity in Refs. [27,28]. Later, they were studied in that context in Ref. [29], and their stability was detailed in Ref. [30]. In Ref. [14] they were briefly considered in the SHG lattice. Our aim here is to give comprehensive results for such solutions. In the following section, they will be extended to the 2D case. We note that, unlike the 1D lattice model with the cubic nonlinearity, in which the TLM disappears in the continuum limit, solitons of this type also exist in the continuum SHG models [34], but they are always unstable [15]. The latter fact suggests that TLM solitons should lose their stability at a finite value of C, as we will verify below.

In the AC limit, one can excite a TLM by setting $v_{n_0}=v_{n_0+1}=\Lambda$ and $u_{n_0}=-u_{n_0+1}=\sqrt{(2\Lambda-k)v_{n_0}}$, while all the other components are zero, cf. Eqs. (13). Continuing the solution branch, we obtain results summarized in Fig. 4. The top panel shows the evolution of the norm of the FF (circles) and SH (stars) components of the TLM soliton vs C. The second and third panels show an example of a TLM for $C=0.1254$ (corresponding to the vertical line in the top panel) and its stability spectrum. It is clear from the third panel that an oscillatory instability (or a Hamiltonian Hopf bifurcation [31]) has arisen in this case ($k=-0.5$ in this case).

The following possibilities have been found for TLMs in the systematic numerical analysis of the stability problem.

(i) For $k<k_{\rm cr}$, where $k_{\rm cr}\approx -0.45$ [this time, the underlying equations were taken in the forms (3) and (4)], there always exists a critical value of the coupling ($C_{\rm cr}\approx 0.1254$ for $k=-0.5$, for example), below which the solution is stable. For $C\geqslant C_{\rm cr}$, the solution is subject to an oscillatory

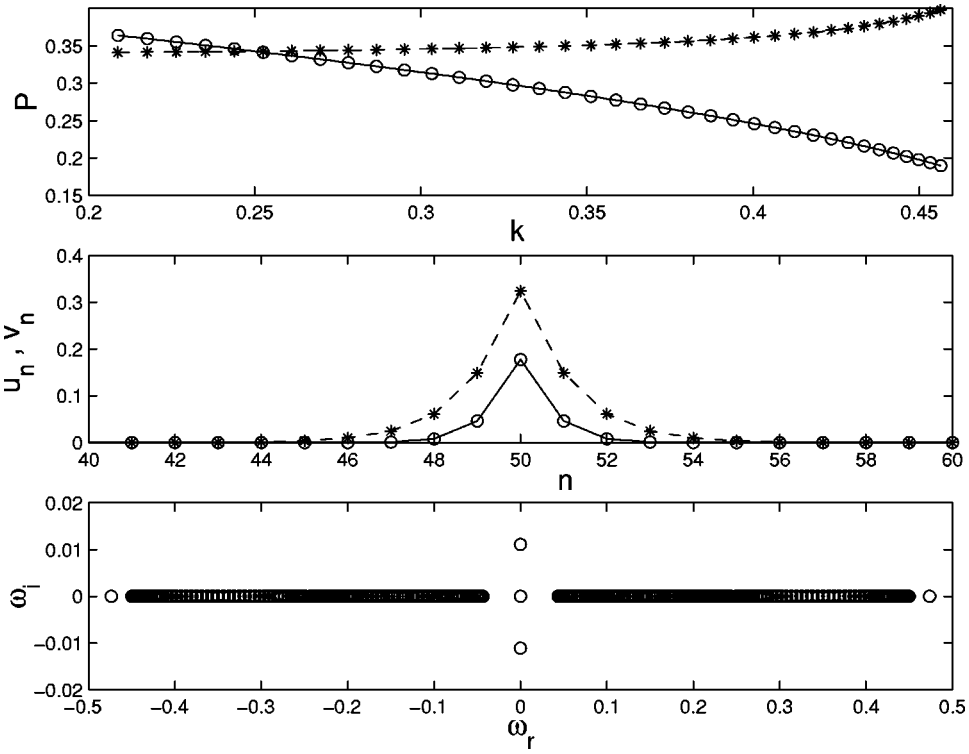

FIG. 3. The evolution of the fundamental soliton with the variation of the mismatch parameter k for $C=0.05$. The top panel shows the norm of the FF (circles) and SH (stars) components vs k. For the final point of the branch ($k\approx 0.456$), the middle panel shows the respective FF and SH spatial profiles, while the bottom one shows the eigenfrequencies of the linearization indicating the presence of an instability of the solution (due to a pair of imaginary eigenfrequencies).

instability, which is generated by a collision of a pair of internal-mode eigenfrequencies that have a negative *Krein sign* [25,32] with the CS (or with a pair of eigenvalues that have bifurcated from the CS). For values $k<k_{\rm cr}$ of the mismatch, we have found the critical value of the coupling constant as a function of k, which is shown in Fig. 5.

(2) For $k_{\rm cr}<k<k_{\rm cr}^{(2)}$, where $k_{\rm cr}^{(2)}\approx -0.005$, there are no oscillatory instabilities. What happens instead, is that the internal eigenmodes do not get close to the CS bands, before pairs of eigenvalues bifurcate from them. Eventually, for $C>C_{\rm cr}$, the interaction between eigenmodes causes the first (internal) pair of eigenfrequencies to exit as imaginary ones (no collision takes place), followed subsequently by the appearance of additional imaginary eigenfrequencies (originating from the modes that bifurcated from the CS). An example of the evolution of the internal-mode eigenvalue for

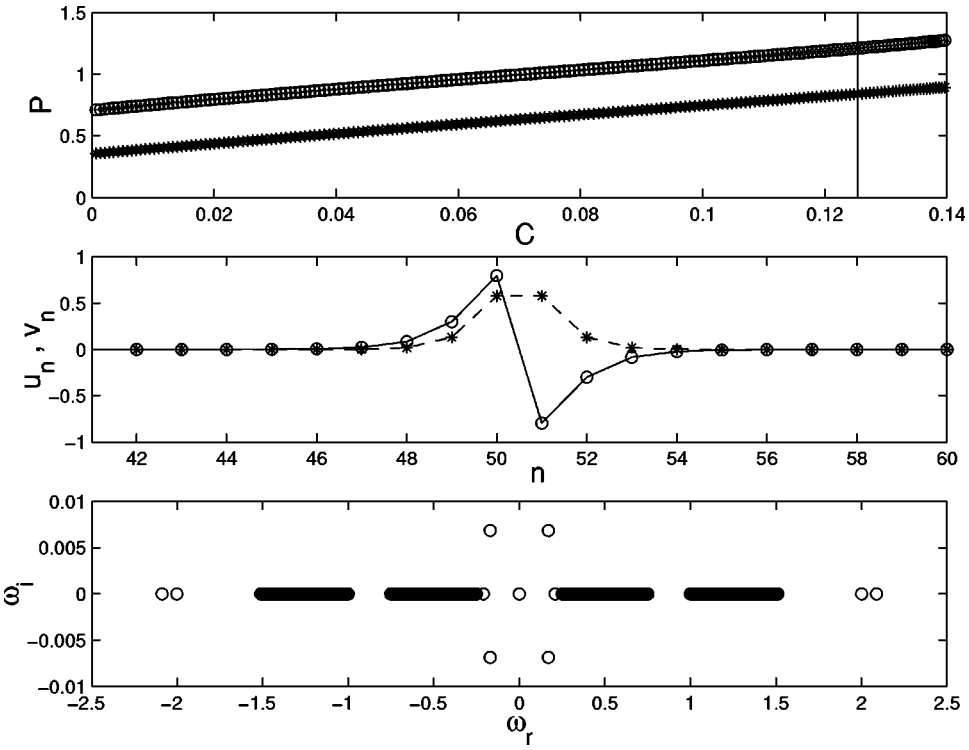

FIG. 4. The figure shows the C dependence of the TLM solution branch, starting from the anticontinuum limit for $k=-0.5$. The top panel demonstrates the variation of the FF (circles) and SH (stars) powers with C. At $C_{\rm cr}=0.1254$ (vertical line in the top panel), the TLM solution is shown in the middle panel (the notation for the FF and SH components is the same as above). The corresponding eigenfrequencies are shown in the lower panel. An oscillatory instability can be clearly discerned.

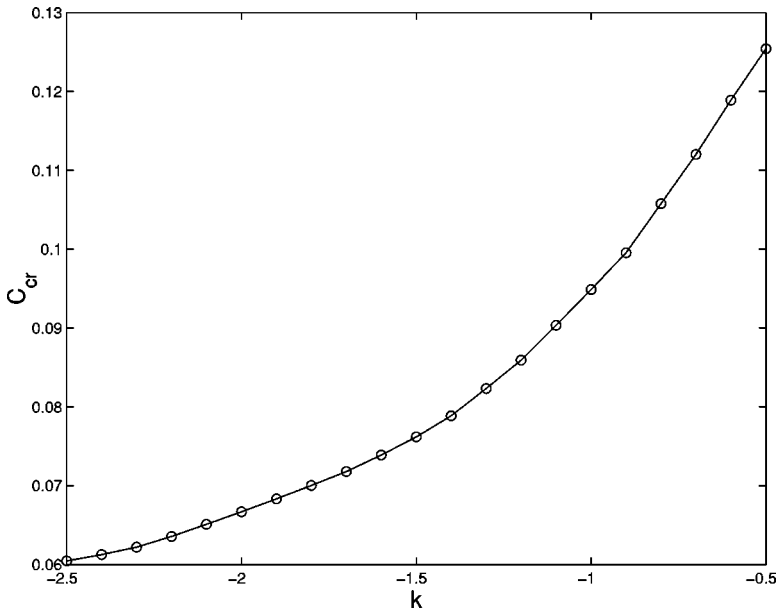

FIG. 5. The critical value $C_{\rm cr}$, such that for $C<C_{\rm cr}$ the TLM soliton is stable, while for $C \geqslant C_{\rm cr}$ a destabilizing Hamiltonian Hopf bifurcation takes place, is shown vs k for $k<k_{cr} \approx -0.45$.

$k=-0.3$ is given in Fig. 6. It can be seen that, despite its initial motion towards the band, the eigenfrequency is ''repelled'' by the modes bifurcating from the CS, and returns to the origin to exit then as an unstable (imaginary) one.

(3) Finally, for $k>k_{\rm cr}^{(2)}$, the TLM's internal modes were shown to be unstable, even for very small C. We do not display detailed results for this case, as the corresponding solitons are definitely unstable (i.e., $C_{\rm cr} \approx 0$).

We also probed the behavior of the internal modes as a function of k for a given coupling constant C, which is shown in Fig. 7. The top panel illustrates a transition of the dominant eigenmode from stability (solid line) to instability (dashed line). An interesting observation to make here is the parabolic approach to the instability, as is seen in the inset [ω^2 scales linearly with $(k-k_{\rm inst})$, where $k_{\rm inst}$ is the value of k for which the instability sets in].

The above features are shared by the two above-mentioned versions of the SHG lattice, based, respectively, on Eqs. (3) and (4), and Eqs. (1) and (2), with $C_1=C_2$ in both cases. However, for the latter model, the values of the parameters at which the same phenomena appear were found to be different from those in the former model. In particular, $k_{\rm cr}$ and $k_{\rm cr}^{(2)}$ were shifted to higher values: in the latter model, $k_{\rm cr} \approx 0.15$ and $k_{\rm cr}^{(2)} \approx 0.25$. Nevertheless, the basic phenomenology of the main regimes remains unaltered.

We have also considered a scenario in which $C_1 \neq C_2$. In particular, since, as it was mentioned above, the SH coupling constant may be smaller than its FF counterpart, we considered the extreme case with $C_2=0$, which is principally different from the above symmetric case with $C_1=C_2$. Here, the phenomenology was found to be somewhat different. A characteristic example can be taken in the region $k<k_{\rm cr}$, where the eigenvalue quartet bifurcates at $C=C_1>C_{\rm cr}$. It was found that, if $C_2=0$, the quartet moved, after the Hamiltonian Hopf bifurcation (which, for instance, occurs at $C=0.0814$ for $k=-0.5$), towards the CS, rather than towards

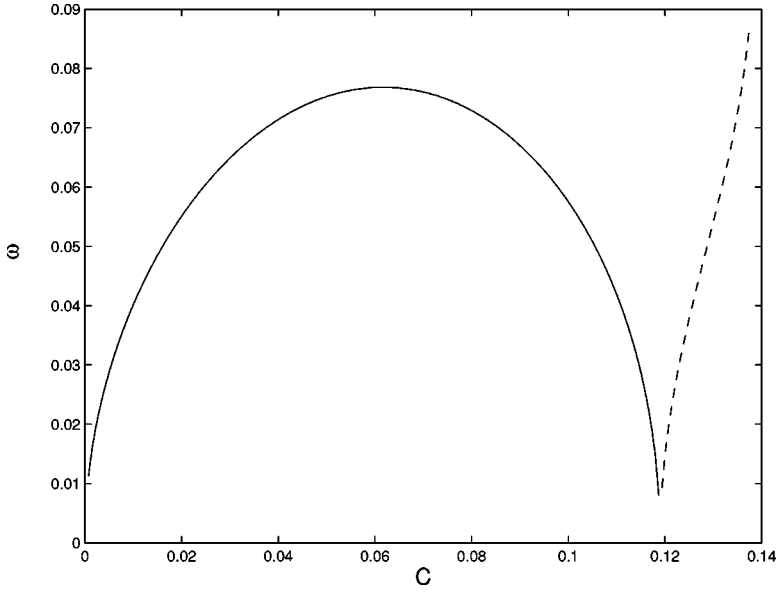

FIG. 6. For $k=-0.3$, such that $k_{\rm cr}<k<k_{\rm cr}^{(2)}$, the evolution of the internal-mode frequency ω is shown vs the coupling constant C for a TLM soliton. After a maximum excursion, the pair of the eigenfrequencies returns to the origin, and then exits as an imaginary one, making the branch unstable. The stable portion of the branch is shown by the solid line, while the dashed one shows the unstable part.

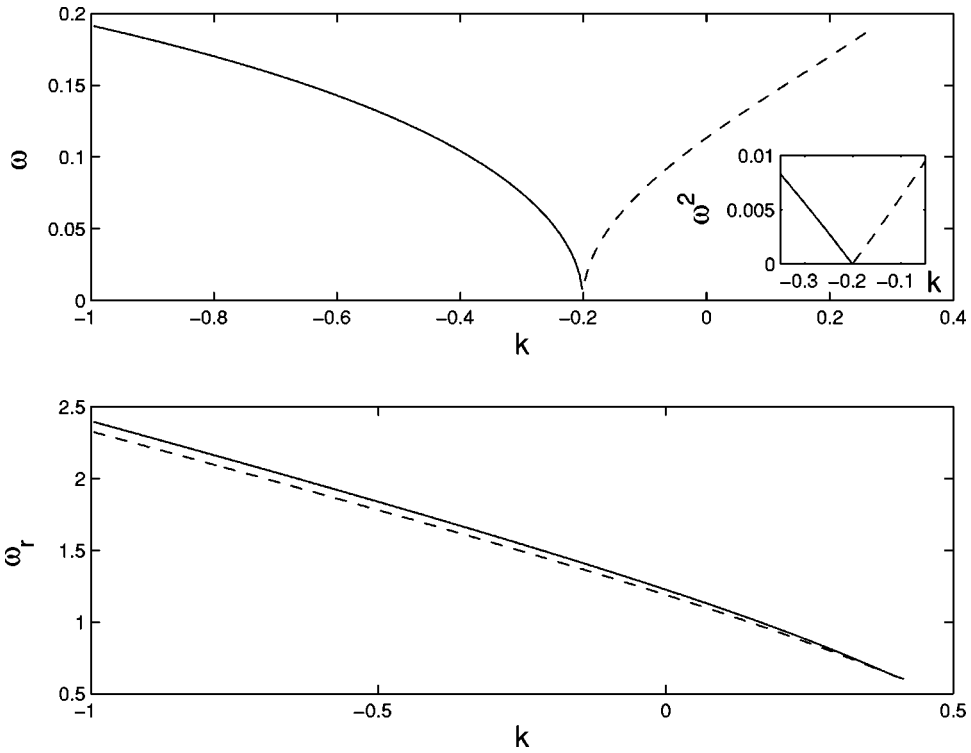

FIG. 7. The continuation of the eigenvalues for fixed $C=0.075$ as a function of k. The top panel shows the internal-mode frequency approaching the origin in the spectral plane (solid line), and then exiting as an unstable eigenfrequency (dashed line). Notice the parabolic approach to the instability border in the inset. The lower panel demonstrates, by means of the solid and dashed lines, the variation of two internal-mode eigenfrequencies above the top edge of the upper continuous spectrum band as a function of k.

the origin as in the previous cases. This resulted in a behavior of the quartet's imaginary part very strongly reminiscent of Fig. 2 in Ref. [33]. The eigenmode with the negative Krein sign [25,32] seeks gaps in the continuous spectrum (that are present due to the finite size of the system for which the numerical computations were done), and approaches them so as to cause restabilization of the branch. This is not possible where the density of states is high (near the band edge), but becomes possible for larger C, as regions of the continuous spectrum with smaller density of states are approached. The details are displayed in Fig. 8. We stress that these results have direct physical meaning, as the real lattice is finite not only in numerical computations but in a physical experiment too. In this case, the computation was performed in domains of $N=100$ sites with periodic boundary conditions (such a case may be quite realistic for experiments with the above-mentioned arrays of optical SHG waveguides).

C. Nonlinear stage of the instability development for the twisted-localized-mode solitons

The natural next step is to simulate the development of the TLM's instabilities of different types within the framework of the full nonlinear model. To this end, we performed

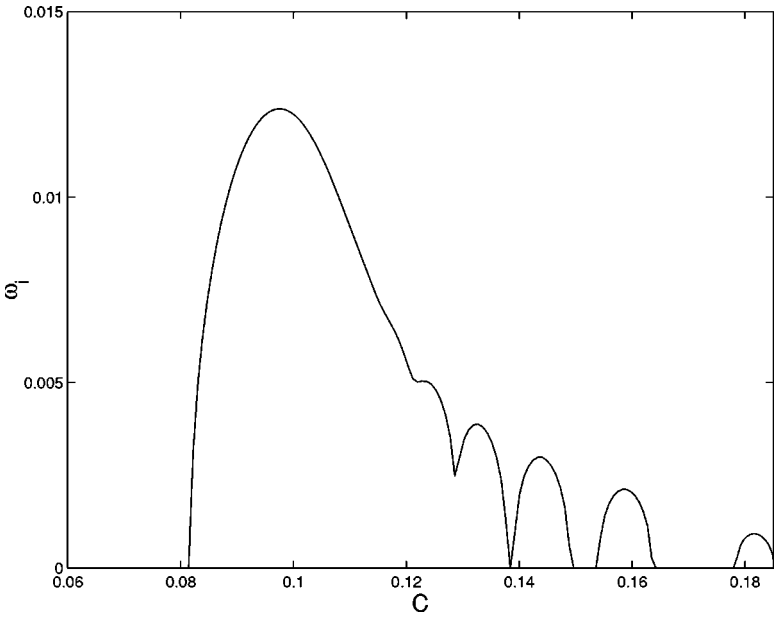

FIG. 8. The evolution of the imaginary part of the quartet eigenvalues (for the TLM soliton) in the case $C_2=0$, $k=-0.5$. It is seen that the instability occurs at $C=0.0814$. However, the quartet does not subsequently move towards the origin in the spectral plain, as it would do for $C_1=C_2$, but rather towards the continuous spectrum. It then attempts to return to the real axis and make the spectrum stable; this is not possible for C close to C_{cr}, but becomes eventually possible for larger values of C. In this computation, $N=100$ nodes have been used, and periodic boundary conditions were imposed.

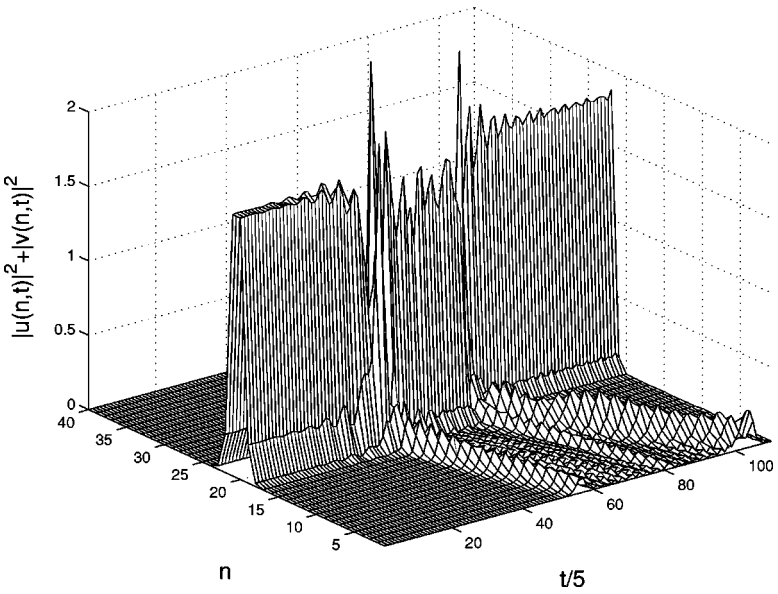

FIG. 9. The temporal evolution of the unstable TLM soliton at $k=-1.5$ and $C=0.15$. The initial TLM configuration was perturbed by a uniformly distributed random field of maximum amplitude 0.005. After a transient period, $0<t<100$, the oscillatory instability transforms the TLM soliton into a (stable) fundamental one. Note that the final pulse is shifted to the left relative to the initial configuration.

direct simulations in the cases of the oscillatory instability, as well as in the case in which the instability stems from imaginary pairs of eigenfrequencies. A typical example for the former case, with $k=-1.5$ and $C=0.15$, is shown in Fig. 9. From the linear stability data displayed in Fig. 5 it follows that the threshold for the Hamiltonian Hopf bifurcation has been crossed, and an unstable quartet of eigenvalues must be present at these values of the parameters. To initiate the growth of the instability, we added a small uniformly distributed random perturbation to the initial solitary-wave configuration. Figure 9 shows the onset of the oscillatory instability after an initial transient of duration $t\approx 100$. The instability does not completely destroy the TLM, but rather rearranges it into a fundamental solution, emitting jets of nonsoliton waves (lattice phonons) in the process. Notice that the resultant fundamental soliton is slightly displaced with respect to the original position of the TLM.

A similar outcome is observed in the case of the instability dominated by the imaginary eigenfrequencies; a typical example is displayed in Fig. 10, which pertains to $k=0.2$ and $C=0.075$. One can see that the initially perturbed TLM is eventually converted into a fundamental soliton, which, however, appears not in a stationary state, but rather with a finite amplitude oscillatory internal mode, excited in the course of the instability-induced conversion.

In all the cases studied, we have observed the transformation of unstable TLM solitons into stable fundamental ones. This outcome seems quite natural, as the fundamental soliton is stable for the corresponding values of the coupling constant and the mismatch parameter.

IV. TWO-DIMENSIONAL SOLITONS

Solitons in the 2D generalization of the SHG lattice are an issue of principal interest, as they may be compared to their earlier studied counterparts in the two-dimensional DNLS equation with the cubic on-site nonlinearity, see Refs. [5] and references therein. It is necessary to stress that no collapse

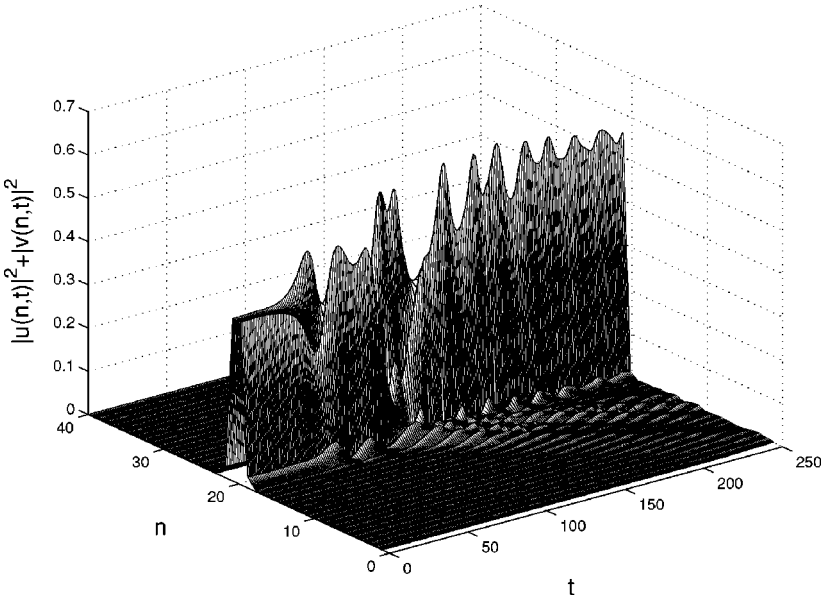

FIG. 10. The same as Fig. 9, but for $k=0.2$ and $C=0.075$, where a pair of purely imaginary eigenfrequencies is responsible for the instability. The instability again results in the conversion of the TLM into a fundamental soliton. Notice the persistent internal oscillations in the emerging pulse.

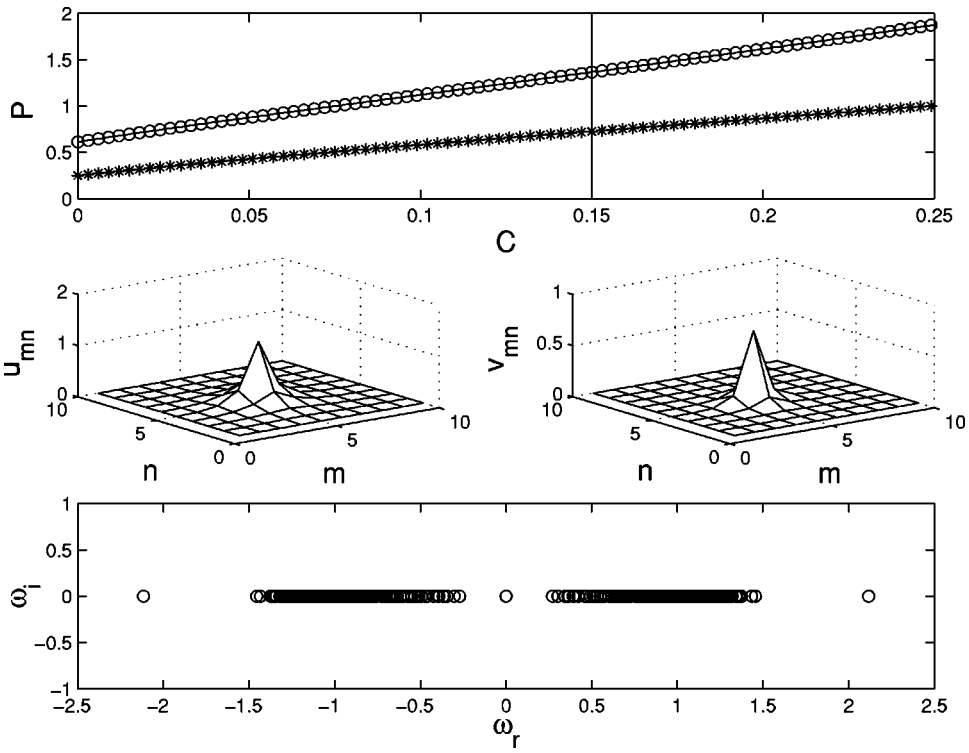

FIG. 11. The 2D fundamental solitons for $k=-0.5$. The top panel shows the powers of the FF (circles) and SH (stars) components of the solution vs C. A typical example of the soliton is shown, for $C=0.15$, in the middle panel; the left and right subplots show the FF and SH fields, respectively. The bottom panel shows the linear stability spectrum for the same case.

occurs in continuum SHG models in two dimensions [35], contrary to what is the case for the NLS equation with the cubic nonlinearity [36]. Due to this fact, solitons (the fundamental ones, without intrinsic vorticity) may be stable in the SHG continuum model in two dimensions [35], even though they are unstable at some values of the parameters (similarly to what was presented in the preceding section for the 1D case).

The 2D equations for the FF and SH fields u_{mn} and v_{mn} differ from Eqs. (1)–(4) by the form of the finite-difference Laplacian: $\Delta_2 u_{mn}=u_{m+1,n}+u_{m-1,n}+u_{m,n+1}+u_{m,n-1}-4u_{mn}$. In line with the above-mentioned facts known for the continuum SHG model in the 2D case, our continuation method, starting from the AC limit, results in a branch of the fundamental-soliton solutions for all values of the coupling C (we also call these solutions zero-spin solitons, as they carry no topological charge, i.e., "spin," S). This branch qualitatively shares the stability features of its 1D counterpart. Examples of the 2D fundamental-soliton solutions are shown in Fig. 11. Even though the solution shown in Fig. 11 is stable, it should be noticed, however, that similarly to 1D, if k is increased for a fixed C, an imaginary eigenvalue bifurcation will eventually occur (see also the discussion in Sec. III A). For example, for $C=0.05$, we have found this bifurcation to occur for $k\approx 0.915$.

The next step is to construct 2D solitons carrying a topological charge ("spin") [22]. It is necessary to mention that spinning solitons are well known in the continuum limit of the SHG model, but, contrary to what is the case for the fundamental solitons, the spinning ones are always strongly unstable against azimuthal perturbations, which break their axial symmetry [37].

A TLM excited in a 2D setting carries a topological charge. Therefore, we will also consider such structures in the two-dimensional setup as another type of 2D solitons. However, since this structure is essentially a bound state of two out-of-phase sites, we will refrain from calling such an entity a vortex.

A regular 2D lattice vortex [22], whose structure emulates both the real and imaginary parts of $\exp(i\theta)$, can be based on a *dual* twisted ansatz [22]. In this case, one TLM is arranged along one lattice direction in the real part of the solution, and another TLM is built along the orthogonal direction in the imaginary part. As it follows from the analysis of the SHG equations (at the AC limit), such a dual structure can be placed only in the FF field. However, the difference from the configuration considered in the previous paragraph is that this time the corresponding SH field emulates the continuum-approximation expression $\cos(2\theta)$, thus carrying spin 2. Given the topological charge of the FF and SH fields, we will symbolize such vortices as $|1,2\rangle$. The unstable spinning solitons of the continuum SHG model [37] are of this type.

We have found that the phenomenology of the 2D TLM, illustrated by Fig. 12, is similar to that described above for its 1D counterpart. In particular, for $k=-0.5$, a destabilizing Hamiltonian Hopf bifurcation, generating a quartet of complex eigenvalues, takes place at $C=C_{\rm cr}^{(2D)}\equiv 0.145$. It is noteworthy that this critical value is larger than its counterpart in the 1D version of the model, $C_{\rm cr}^{(1D)}=0.125$.

We also considered the development of the oscillatory instability of the TLM solutions in the 2D setting. A typical example is shown in Fig. 13 for $k=-0.5$ and $C=0.249$. The initial configuration (not shown here) is a TLM with two out-of-phase, next-nearest-neighbor peaks in the FF, and in-phase, next-nearest-neighbor peaks in the SH field. One can

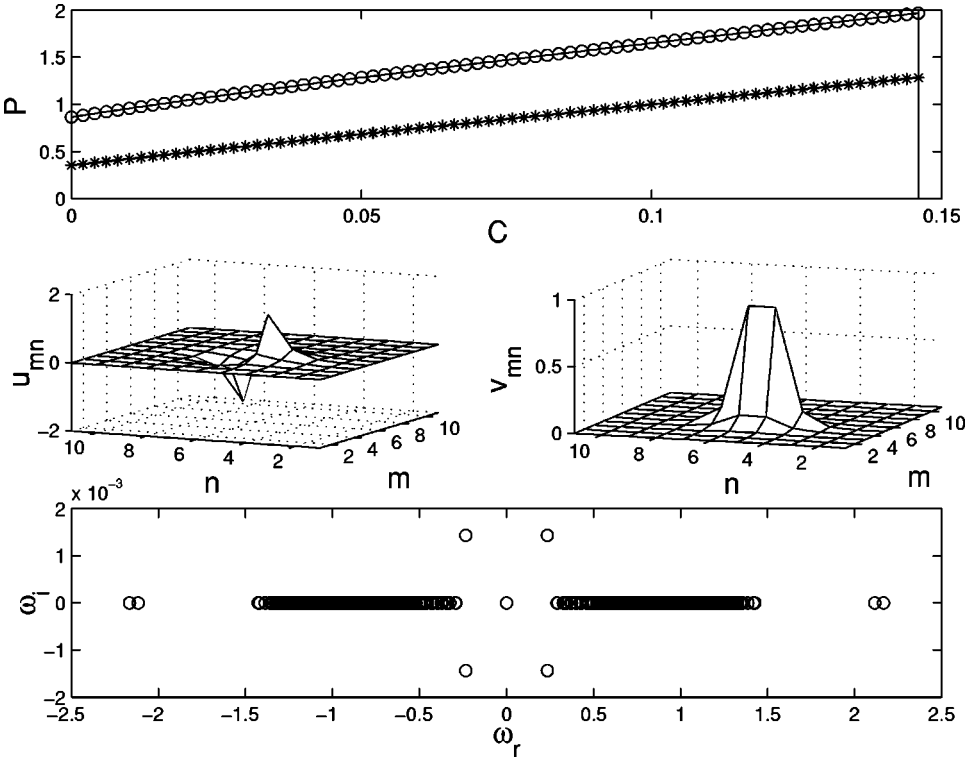

FIG. 12. The branch of the two-dimensional TLM solutions, found at $k=-0.5$. The top plot shows, as in the previous figures, the norms of the FF and SH components of the solution vs C. The middle subplot shows an example of the FF (left) and SH (right) components of the TLM for $C=0.145$ (close to the onset of the oscillatory instability). The lower subplot shows the corresponding eigenfrequencies, indicating the presence of such an instability.

observe that the oscillatory instability starts to develop after $t\approx 50$, and eventually leads to a single-humped solution, shown for $t\approx 95$ in the top panels of Fig. 13. The bottom panels show the development of the instability (which starts after approximately two oscillations with the FF period $T=8\pi$) for some of the central sites of the configuration. This result of the instability was found to be typical, and can be naturally expected on the basis of arguments similar to those presented in Sec. III for the 1D problem.

The $|1,2\rangle$ vortex-solution branch demonstrates a somewhat similar phenomenology, but with a greater variety of potential instabilities. An example of the $|1,2\rangle$ vortex is displayed in Fig. 14 for $k=0.25$ and $C=0.1$. The solutions of this type become unstable due to a quartet bifurcation at $C=C_{\rm cr}^{(1)}=0.119$. Subsequent increase of the coupling C induces further instabilities, which set in at $C=C_{\rm cr}^{(2)}=0.138$, and then at $C=C_{\rm cr}^{(3)}=0.161$. An example of the eigenvalue spectrum is shown, for $C=0.19$, in Fig. 15, where the presence of three quartets of complex eigenvalues is evident. It should be highlighted, however, that the stability (for $C<C_{\rm cr}^{(1)}$) of this branch with $S=2$ in its SH field can be contrasted to the case of cubic nonlinearity, where such solutions were always found to be unstable [22].

In all the cases considered, it was found that the net to-

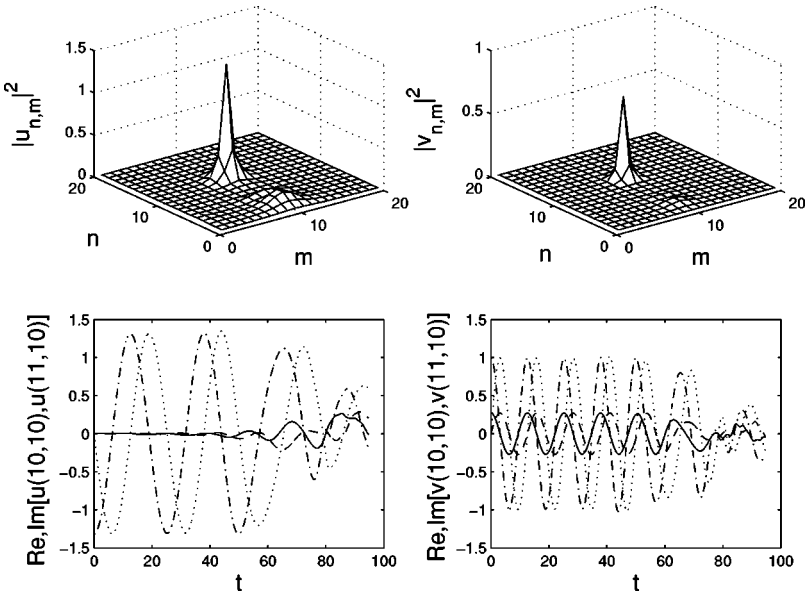

FIG. 13. An example of the instability of the 2D TLM solution (used as an initial condition for the time integration) for $k=-0.5$, $C=0.249$, and $\Lambda=0.25$. The two top panels show final two-dimensional spatial profiles of the FF and SH fields (at $t=94.65$). It is clearly seen that a symmetry-breaking instability has occurred, resulting in the establishment of the single-humped solution, which is stable. The two bottom panels show the time evolution of two of the central-most sites of the configuration for the FF (bottom left) and SH (bottom right) fields. The solid line in both cases shows the real part of the field at the site $(n,m)=(10,10)$, the dashed line shows the imaginary part at (10,10), the dash-dotted line is the real part at $(n,m)=(11,10)$, while the dotted line shows the imaginary part of the field at (11,10).

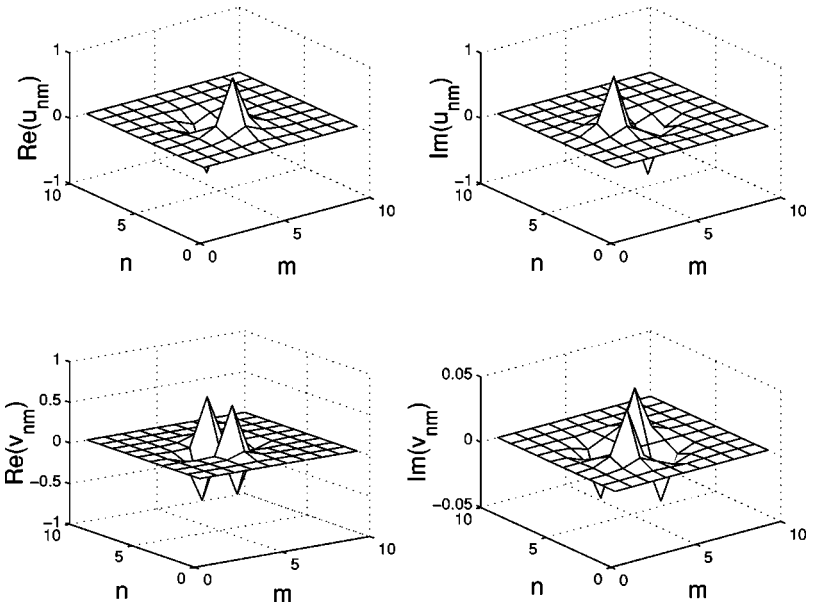

FIG. 14. An example of the $|1,2\rangle$ vortex, found for $C=0.1$ and $k=0.25$. This solution is stable. Shown are the real and imaginary parts of the FF field (in the top left and right panels, respectively) and the same for the SH field (the bottom left and right panels, respectively).

pological charge in both FF and SH components of the solution coincided with the number of eigenfrequencies having the negative Krein sign in the eigenvalue spectrum. This observation suggests a conjecture that the net vorticity (in both components of the vortex) gives the number of possible different oscillatory instabilities (or, in other words, the maximum possible number of eigenvalue quartets). Note that, if a phase change of π across the soliton in the 1D lattice is considered as the soliton's topological charge, this conjecture is also true for the 1D TLM solutions, which were considered in the preceding section (their topological charge is then 1 and 0 in the FF and SH components, respectively).

V. CONCLUSION

We have considered many families of solitary waves in the one- and two-dimensional discrete second-harmonic-generating model. The stability of fundamental solitons was analyzed in both dimensions. We have also studied twisted-mode solitons for which there always exists an instability threshold, which was identified in the one-dimensional lattice. Similar stability thresholds have been found for solitons with a topological charge of the types $|1,0\rangle$ and $|1,2\rangle$ (the latter one may be interpreted as a discrete vortex) in the 2D lattice. In the case when the one-dimensional twisted-mode solitons, or two-dimensional topologically charged ones, are unstable, direct simulations have demonstrated that the instability, which may be due to either a complex or purely imaginary pair of eigenfrequencies, initiates transformation of the unstable soliton into a stable fundamental one, which is possible as the topological charge is not conserved in discrete systems.

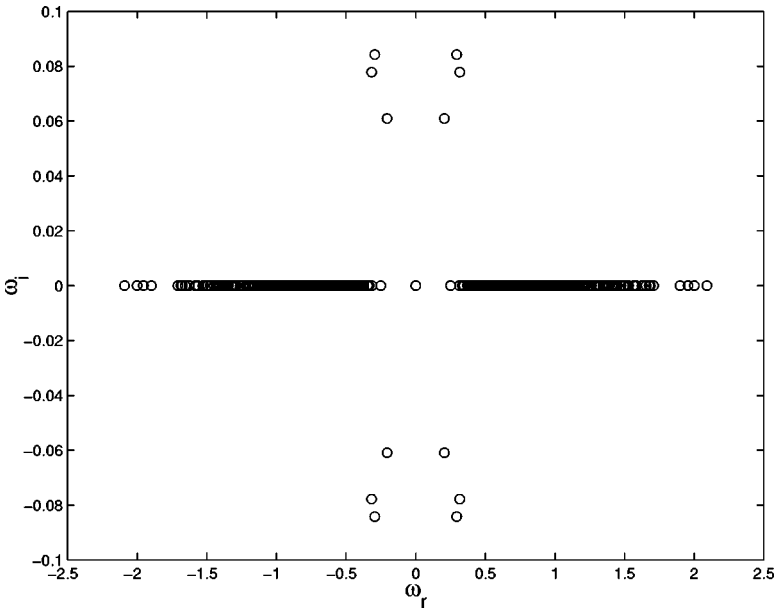

FIG. 15. The linear stability spectrum for the vortexlike state of $|1,2\rangle$ type at $k=0.25$ and $C=0.19$. There are three eigenvalues with the negative Krein sign, which give rise, after collisions with the continuous spectrum, to three eigenvalue quartets.

ACKNOWLEDGMENTS

B.A.M. and P.G.K. appreciate the hospitality of the Max-Planck Institute for Physics of Complex systems in Dresden (Germany). P.G.K. also gratefully acknowledges partial support from the University of Massachussetts through a faculty research grant.

[1] A. J. Sievers and S. Takeno, Phys. Rev. Lett. **61**, 970 (1988).
[2] J. B. Page, Phys. Rev. B **41**, 7835 (1990).
[3] S. Flach and C. R. Willis, Phys. Rep. **295**, 181 (1998).
[4] S. Aubry, Physica D **103**, 201 (1997).
[5] P. G. Kevrekidis, K. Ø. Rasmussen, and A. R. Bishop, Int. J. Mod. Phys. B **15**, 2833 (2001).
[6] U. T. Schwarz, L. Q. English, and A. J. Sievers, Phys. Rev. Lett. **83**, 223 (1999).
[7] B. L. Swanson, J. A. Brozik, S. P. Love, G. F. Strouse, A. P. Shreve, A. R. Bishop, W.-Z. Wang, and M. I. Salkola, Phys. Rev. Lett. **82**, 3288 (1999).
[8] H. Eisenberg, Y. Silberberg, R. Morandotti, A. R. Boyd, and J. S. Aitchison, Phys. Rev. Lett. **81**, 3383 (1998).
[9] R. Morandotti, U. Peschel, J. S. Aitchison, H. S. Eisenberg, and Y. Silberberg, Phys. Rev. Lett. **83**, 2726 (1999).
[10] E. Trias, J. J. Mazo, and T. P. Orlando, Phys. Rev. Lett. **84**, 741 (2000).
[11] P. Binder, D. Abraimov, A. V. Ustinov, S. Flach, and Y. Zolotaryuk, Phys. Rev. Lett. **84**, 745 (2000).
[12] D. N. Christodoulides and R. I. Joseph, Opt. Lett. **13**, 794 (1988); A. Aceves, C. De Angelis, S. Trillo, and S. Wabnitz, *ibid.* **19**, 332 (1994); A. Aceves, C. De Angelis, G. G. Luther, and A. M. Rubenchik, *ibid.* **19**, 1186 (1994); A. Aceves *et al.*, Phys. Rev. Lett. **75**, 73 (1995); A. Aceves and M. Santagiustina, Phys. Rev. E **56**, 1113 (1997).
[13] A. Campa and A. Giansanti, Phys. Rev. E **58**, 3585 (1998).
[14] S. Darmanyan, A. Kobyakov, and F. Lederer, Phys. Rev. E **57**, 2344 (1998).
[15] C. Etrich, F. Lederer, B. A. Malomed, T. Peschel, and U. Peschel, Prog. Opt. **41**, 483 (2000).
[16] V. M. Agranovich, O. A. Dubovskii, and A. V. Orlov, Solid State Commun. **72**, 491 (1989).
[17] O. A. Dubovskii and A. V. Orlov, Phys. Solid State **41**, 642 (1999); V. M. Agranovich, O. A. Dubovsky, A. M. Kamchatnov, and P. Reineker, Mol. Cryst. Liq. Cryst. Sci. Technol., Sect. A **355**, 25 (2001).
[18] V. V. Konotop and B. A. Malomed, Phys. Rev. B **61**, 8618 (2000).
[19] O. Bang, P. L. Christiansen, and C. B. Clausen, Phys. Rev. E **56**, 7257 (1997).
[20] A. A. Sukhorukov, Yu. S. Kivshar, O. Bang, and C. M. Soukoulis, Phys. Rev. E **63**, 016615 (2001).
[21] See Ref. [4] and M. Johansson, S. Aubry, Yu. B. Gaididei, P. L. Christiansen, and K. Ø. Rasmussen, Physica D **119**, 115 (1998).
[22] B. A. Malomed and P. G. Kevrekidis, Phys. Rev. E **64**, 026601 (2001).
[23] D. E. Pelinovsky, A. V. Buryak, and Y. S. Kivshar, Phys. Rev. Lett. **75**, 591 (1995).
[24] C. Etrich, U. Peschel, F. Lederer, B. A. Malomed, and Yu. S. Kivshar, Phys. Rev. E **54**, 4321 (1996).
[25] M. Johansson and S. Aubry, Phys. Rev. E **61**, 5864 (2000).
[26] P. G. Kevrekidis, K. Ø. Rasmussen, and A. R. Bishop, Math. Comput. Simul. **55**, 449 (2001).
[27] E. W. Laedke, O. Kluth, and K. H. Spatschek, Phys. Rev. E **54**, 4299 (1996).
[28] M. Johansson and S. Aubry, Nonlinearity **10**, 1151 (1997).
[29] S. Darmanyan, A. Kobyakov, and F. Lederer, JETP **86**, 682 (1998).
[30] P. G. Kevrekidis, A. R. Bishop, and K. Ø. Rasmussen, Phys. Rev. E **63**, 036603 (2001).
[31] J.-C. van der Meer, Nonlinearity **3**, 1041 (1990); I. V. Barashenkov, D. E. Pelinovsky, and E. V. Zemlyanaya, Phys. Rev. Lett. **80**, 5117 (1998); A. De Rossi, C. Conti, and S. Trillo, *ibid.* **81**, 85 (1998).
[32] P. G. Kevrekidis and T. Kapitula (unpublished).
[33] M. Johansson and Yu. S. Kivshar, Phys. Rev. Lett. **82**, 85 (1999).
[34] M. J. Werner and P. D. Drummond, J. Opt. Soc. Am. B **10**, 2390 (1993).
[35] V. V. Steblina, Yu. S. Kivshar, M. Lisak, and B. A. Malomed, Opt. Commun. **118**, 345 (1995); A. V. Buryak, Yu. S. Kivshar, and V. V. Steblina, Phys. Rev. A **52**, 1670 (1995).
[36] C. Sulem and P. L. Sulem, *The Nonlinear Schrödinger Equation: Self-focusing and Wave Collapse* (Springer-Verlag, New York, 1999).
[37] W. J. Firth and D. Skryabin, Phys. Rev. Lett. **79**, 2450 (1997); D. V. Petrov and L. Torner, Opt. Quantum Electron. **29**, 1037 (1997).